

1 **ERCC1 mice, unlike other premature aging models, display accelerated epigenetic**
2 **age**

3

4 Kevin Perez^{1,2}, Alberto Parras^{1,2}, Cheyenne Rechsteiner¹, Amin Haghani³, Robert Brooke⁴,
5 Calida Mrabti¹, Lucas Schonfeldt¹, Steve Horvath^{3,4,5}, Alejandro Ocampo^{1,10}

6

7 ¹Department of Biomedical Sciences, Faculty of Biology and Medicine, University of
8 Lausanne, Lausanne, Switzerland.

9 ³Altos Labs, San Diego, USA

10 ⁴Epigenetic Clock Development Foundation, Torrance, CA, USA

11 ⁵Human Genetics, David Geffen School of Medicine, University of California, Los Angeles,
12 USA

13

14 ²These authors contributed equally.

15 ¹⁰Lead contact.

16 Correspondence: alejandro.ocampo@unil.ch

17

18 **Keywords:** progeria, epigenetic clock, methylation, DNA damage, accelerated aging

19 **ABSTRACT**

20 Over the last decades, several premature aging mouse models have been developed to
21 study aging and identify interventions that can delay age-related diseases. Yet, it is still
22 unclear whether these models truly recapitulate natural aging. Here, we analyzed DNA
23 methylation in multiple tissues of four previously reported mouse models of premature aging
24 (ERCC1, LAKI, POLG and XPG). We estimated DNA methylation (DNAm) age of these
25 samples using the Horvath clock. The most pronounced increase in DNAm age could be
26 observed in ERCC1 mice, a strain which exhibits a deficit in DNA nucleotide excision repair.
27 In line with these results, we detected an increase in epigenetic age in fibroblasts isolated
28 from patients with progeroid syndromes associated with mutations in DNA excision repair
29 genes. These findings highlight ERCC1 as a particularly attractive mouse model to study
30 aging in mammals and suggest a strong connection between DNA damage and epigenetic
31 dysregulation during aging.

32

33 **MAIN TEXT**

34 The world's population is growing older. Since aging represents the strongest risk factor for
35 most human diseases, it is therefore key to identify anti-aging interventions that could delay
36 or even reverse the aging process¹. Towards this goal, several accelerated aging mouse
37 models have been developed to study the aging process^{2,3}, some of them stemming from
38 existing human disorders^{4,5}. In this line, premature aging rodents could speed up the
39 discovery of anti-aging interventions by shortening the experimental time, but only if the
40 results can be translatable to natural aging. Nevertheless, the physiological relevance of
41 these models and whether they truly recapitulate or phenocopy natural aging remains
42 controversial. Epigenetic changes are one of several hallmarks of aging in numerous
43 organisms⁶. The importance of epigenetic changes in mammals has been reinforced by the
44 development of epigenetic clocks that can accurately estimate age in multiple tissues and all
45 mammalian species⁷⁻¹¹. Interestingly, several anti-aging interventions have been shown to
46 reverse these clocks¹², including cellular reprogramming¹³⁻¹⁶. Here, we sought to assess the
47 relevance of several premature aging mouse models to study aging. Toward this end, we
48 analyzed mouse models of segmental progeria by assessing the epigenetic age of multiple
49 tissues and organs using epigenetic clocks based on DNA methylation.

50

51 Specifically, we analyzed the epigenetic age ("Horvath Pan Tissue clock")¹⁷ of five tissues of
52 four commonly used premature aging models including: ERCC1, XPG, LAKI and POLG
53 mice. These mouse strains cause premature aging through various biological mechanisms
54 by carrying mutations that lead to the manipulation of different hallmarks of aging.
55 Specifically, ERCC1¹⁸ and XPG¹⁹ mice exhibit a deficit in nucleotide excision repair (NER) of
56 the nuclear DNA, POLG mice show accumulation of mitochondrial DNA mutations^{20,21} and
57 lastly LMNA knock-in (LAKI) mice suffer nuclear lamina defects^{22,23}. To perform comparative
58 studies in these strains, we assessed the DNA methylation age (DNAm) in ERCC1^{KO/Δ},
59 XPG^{KO/KO}, LAKI^{TG/TG} and POLG^{TG/TG} mice at several timepoints including during post-natal
60 development, at median survival, and in old age, relative to each model's own lifespan. Both

61 proliferative (blood and skin) and more terminally differentiated tissues (liver, cerebral cortex,
62 and skeletal muscle) were analyzed at these ages (Figure 1a). During the generation of
63 experimental mice, we noticed that while LAKI^{TG/TG} and POLG^{TG/TG} mice were born at a
64 predicted Mendelian frequency, ERCC1^{KO/Δ} and XPG^{KO/KO} showed a perinatal lethality
65 (Figure S1a). Furthermore, as previously reported the four premature aging animals were
66 significantly smaller and exhibited reduced body weight compared to their control littermates
67 as expected (Figure 1b). Before analyzing the progeria models, we first looked at the clock
68 performance in the control littermate WT mice (C57BL6J and C57BL6J|FVB hybrid
69 backgrounds), a quality check that methylation can accurately predict chronological age in
70 multiple tissues. The chronological age prediction in these two different backgrounds was
71 highly accurate in blood (C57BL6J, RMSE: 2.08wk, r = 0.99; C57BL6J|FVB, RMSE: 2.55wk,
72 r = 0.95) and provided sufficient accuracy in the other tissues (Figure S1b and Table S1),
73 confirming the precision of the DNAm clock to predict age, particularly in blood. Next, we
74 determined the DNAm age in the five tissues of ERCC1^{KO/Δ}, LAKI^{TG/TG} and XPG^{KO/KO} at 8
75 weeks, and POLG^{TG/TG} at 30 weeks of age corresponding to the relative median survival of
76 the strain. Strikingly, ERCC1^{KO/Δ} was the only premature aging model where we observed
77 increased biological age compared to control littermates (Figure 1c). Importantly, the
78 biological age of ERCC1^{KO/Δ} mice was most increased in blood [WT: 6.85w (1.62), KO/Δ:
79 12.46w (1.08)], but was also significantly increased in brain, liver, skeletal muscle and skin,
80 tissues and organs known to be affected in this mouse model. Conversely, we did not detect
81 any acceleration in DNAm age at 8 weeks in LAKI or XPG mice, nor in POLG mice at 30
82 weeks in any tissue (Figure 1c). This result indicates that only ERCC1 aging mouse model
83 shows a significant increase in epigenetic age at the median lifespan.

84

85 Subsequently, and with the goal of confirming this observation, we analyzed the methylation
86 age at different times points during the lifespan of the mice including, ERCC1^{KO/Δ} (2, 8 and
87 20 weeks), LAKI^{TG/TG} (8 and 23 weeks), and POLG^{TG/TG} (30 and 47 weeks). Interestingly, in
88 the ERCC1^{KO/Δ} mice, biological age was increased mildly at 2 weeks old in blood, but not in

89 other tissues. However, at 20 weeks, DNAm age was significantly accelerated in blood, liver,
90 and skin (Figure 2a and Table S2). Conversely, as we observed at earlier timepoints, DNAm
91 age was not changed in any of the analyzed tissues at 14.4 weeks in LAKI^{TG/TG} mice, nor in
92 POLG^{TG/TG} mice at 47 weeks (Figure S1c). Together, our results further confirm that the
93 biological age measured by DNA methylation is increased only in the ERCC1 mouse model
94 of premature aging, at multiple ages, with blood being the tissue with the strongest statistical
95 power. Importantly, when the same analysis was restricted to either male or female only, the
96 same trend appeared, with increased DNAm age primarily in the ERCC1 mouse model.
97 Next, we wondered whether the observed differences between methylation age and
98 chronological age in ERCC1 mice were constant or changed throughout life. To determine
99 this accelerated aging rate, we calculated the slope between biological and chronological
100 age in each tissue in ERCC1 +/+ vs. KO/ Δ mice. Importantly, the rate was significantly
101 different in blood (Slope: WT = 0.78, KO/ Δ = 1.29), skeletal muscle (Slope: WT = 0.84, KO/ Δ
102 = 1.17) and brain (Slope: WT = 0.91, KO/ Δ = 1.2) (Figure 2b), demonstrating that the
103 difference between biological and chronological age increased during life in ERCC1^{KO/ Δ}
104 mice.

105

106 Lastly, to investigate the potential relevance of these findings to human patients, we
107 analyzed the DNAm age of samples obtained from patients affected by diseases caused by
108 mutations in DNA excision repair genes associated with aging phenotypes: Xeroderma
109 Pigmentosum (XP) affecting *ERCC5*²⁴, and Cockayne Syndrome (CS) type A (CSA)
110 affecting *ERCC8* and type B (CSB) affecting *ERCC6*²⁵. Towards this goal, we profiled DNAm
111 age from fibroblasts derived from patients at multiple ages: control (1, 5, 11-year-old), CSA
112 (1, 3, 5-year-old), CSB (3, 8, 10-year-old), XP (1, 2, 5-year-old). For this analysis only, we
113 selected the DNAm age from the “Skin&Blood” Clock, as this has previously been shown to
114 be more accurate than the “PanTissue” clock to assess age of human fibroblasts²⁶, a finding
115 that we also confirmed in our own dataset (Figure 3a). Importantly, the DNAm age was
116 significantly higher in the affected patients compared to control samples (Figure 3a). Finally,

117 we calculated the difference between DNAm age and chronological age for each sample,
118 detecting a significant increase for the XP patients and a strong tendency in the rest of the
119 disease samples (Figure 3b). Overall, these results indicate that human progeroid
120 syndromes associated with mutations in DNA excision repair genes display accelerated
121 epigenetic age.

122

123 Although premature aging models have been widely used to study aging and evaluate anti-
124 aging interventions, their physiological relevance for the study of aging has not been deeply
125 investigated. Here, we analyzed the biological age (“Horvath clock”) of four premature aging
126 mouse models (ERCC1, POLG, XPG, LAKI) and demonstrated that only ERCC1 mice truly
127 shows accelerated aging.

128

129 Depletion of ERCC1 protein results in a defect in DNA repair, leading to an accumulation of
130 DNA mutations in multiple tissues and organs. Importantly, DNA damage has been
131 proposed as one of the most central hallmarks of aging, as well as a causative driver^{27,28}.
132 Here, we show that a defective DNA repair mechanism leads to epigenetic aging, strongly
133 suggesting a link between DNA damage and epigenetic dysregulation. Interestingly, dietary
134 restriction, the most robust anti-aging intervention, dramatically extends lifespan of
135 ERCC1^{KO/Δ} mice²⁹ and knocking down of *ERCC1* gene in blood specifically causes
136 premature aging³⁰. Furthermore, we noted that even though DNAm age was increased in
137 ERCC1 mice already at 2 weeks, greater changes were observed in older animals indicating
138 a progressive age acceleration during aging. In this line, we postulate that a higher DNA
139 repair capacity during development³¹ or embryonic reprogramming programs, which might
140 prevent potential epigenetic dysregulation as consequence of DNA damage, could protect
141 the animals during gestation. Taken together, these results suggest that ERCC1 mice stand
142 perhaps as one of the most relevant mouse models of premature aging.

143

144 The methylation clock was more accurate in blood, a rapidly proliferative tissue that
145 undergoes constant regeneration, in which the most significant and strongest differences
146 between ERCC1 and control mice were observed. Therefore, due to its easy collection and
147 strong sensitivity for epigenetic aging, we propose the use of blood as one of the best
148 choices to study and analyze the effect of anti-aging interventions. Lastly, although multiple
149 groups have examined the biological age of human diseases associated with premature
150 aging, no changes in DNAm age have been observed in the blood of Hutchinson-Gilford
151 progeria syndrome patients³². On the other hand, a significant increase in biological age was
152 seen in samples from Werner³³, Down syndrome even in newborns³⁴ in several human
153 overgrowth syndromes including Sotos syndrome³⁵ and Tatton-Brown-Rahman syndrome³⁶
154 and very recently in Leigh Syndrome and mitochondrial encephalopathy with lactic acidosis
155 and stroke-like episodes (MELAS) patients³⁷. Other studies have identified changes in
156 DNAm in premature aging models, independent of the DNA methylation clocks³⁸⁻⁴⁰. Our
157 survey of mouse models of premature aging may be expanded to alternative premature
158 aging models², or additional tissues and timepoints. Likewise, it would be interesting to also
159 assess biological age using newly developed clocks, such as transcriptomic, proteomic or
160 chromatin accessibility clocks⁴¹⁻⁴³.

161

162 **ACKNOWLEDGMENTS**

163 We would like to thank all members of the Ocampo laboratory for helpful discussions. We
164 would like to thank the teams of mouse facilities at the University of Lausanne including
165 Francis Derouet and Lisa Arlandi (animal facility at Epalinges), and Laurent Lecomte (animal
166 facility of the Department of Biomedical Sciences) and colleagues. We thank Prof. Jan
167 Hoeijmakers and Prof. Ingrid van der Pluijm for providing us the ERCC1 and XPG mice, and
168 Prof. Carlos Lopez Otin and Prof. Andrea Ablasser for providing us the LAKI mice.

169 This work was supported the Swiss National Science Foundation (SNSF), the University of
170 Lausanne, and the Canton Vaud.

171

172 **CONFLICT OF INTEREST**

173 S.H. is a founder of the non-profit Epigenetic Clock Development Foundation which licenses
174 several patents from his former employer UC Regents. These patents list S.H. as inventor.
175 The other authors declare no conflicts of interest.

176

177 **AUTHOR CONTRIBUTIONS**

178 K.P. performed data and statistical analysis. A.P. generated mouse strains and collected
179 tissues. C.M and L.S. were involved in culture and DNA extraction from human cells. C.R.
180 extracted DNA from mice. S.H., A.H. analyzed data and made a critically revision. A.O.
181 directed, supervised the study, designed the experiments, and reviewed the manuscript.
182 K.P. and A.P generated the figures and wrote the manuscript with input from all authors.

183

184 **DATA AVAILABILITY STATEMENT**

185 The data supporting the findings of this study are available from the corresponding author
186 upon reasonable request.

187 The mammalian methylation array is available from the nonprofit Epigenetic Clock
188 Development Foundation (<https://clockfoundation.org/>)

189

190

191 **FIGURE LEGENDS**

192 **FIGURE 1. DNA methylation in premature aging mouse models. (a)** Schematic
193 representation of premature mouse strains and littermate controls, tissues collected, and
194 timepoints taken. **(b)** Evolution of body weight (grams) of mutant and controls mice from 4
195 weeks until the euthanize point, data are mean \pm SEM. **(c)** Methylation biological age (in
196 weeks) of ERCC1^{KO/ Δ} , XPG^{KO/KO}, LAK1^{TG/TG} at 8 weeks and POLG^{TG/TG} at 30 weeks. Data
197 are represented as box plots (center line shows median, box shows 25th and 75th
198 percentiles and whiskers show minimum and maximum values and statistical significance
199 was assessed by two-sided unpaired t-test.

200

201 **FIGURE 2. DNA methylation ERCC1 mice. (a)** Methylation biological age (in weeks) of
202 ERCC1^{KO/Δ} mice at 2, 8 and 20 weeks in multiple organs/tissues and WT littermate controls
203 estimated by Horvath clock. Data are represented as box plots (center line shows median,
204 box shows 25th and 75th percentiles and whiskers show minimum and maximum values and
205 statistical significance was assessed by two-sided unpaired t-test. **(b)** Slope of aging in
206 ERCC1^{KO/Δ} and controls mice in tissues analyzed from 2 to 20 weeks old. Significance of the
207 interaction term in the linear regression was analyzed.

208

209 **FIGURE 3. DNA methylation in fibroblasts from human premature aging diseases. (a)**
210 DNAm age versus chronological age (in years) and **(b)** difference between biological and
211 chronological age in human samples in fibroblasts isolated from individual with Cockayne
212 Syndrome A (CSA), Cockayne Syndrome B (CSB), Xeroderma Pigmentosum (XP) and
213 controls analyzed by Skin&Blood Clock. Data are represented as box plots (center line
214 shows median, box shows 25th and 75th percentiles and whiskers show minimum and
215 maximum values and statistical significance was assessed by two-sided unpaired t-test.

216

217 **SUPPLEMENTARY FIGURE 1. DNA methylation in premature aging mouse models**
218 **additional data. (a)** Breeding protocol to generate the four premature mouse strains and
219 littermate control mice. Statistical significance was assessed by Pearson's chi-squared test.
220 **(b)** Correlation between biological and chronological age (in weeks) in WT control mice in
221 C57BL6J and C57BL6J|FVB backgrounds in analyzed tissues from 2- to 47-week-old. **(c)**
222 Methylation biological age of POLG^{TG/TG} (at 30 and 47 weeks old) and LAK1^{TG/TG} (at 8 and 23
223 weeks) in multiple organs/tissues and WT littermate controls by Horvath clock. Data are
224 represented as box plots (center line shows median, box shows 25th and 75th percentiles
225 and whiskers show minimum and maximum values) and statistical significance was
226 assessed by two-sided unpaired t-test.

227

228 **EXPERIMENTAL PROCEDURES**

229 **Animal housing**

230 All the experimental experiment were performed in accordance with Swiss legislation after
231 the approval from the local authorities (Cantonal veterinary office, Canton de Vaud,
232 Switzerland). Mice were housed in groups of five per cage with a 12hr light/dark cycle
233 between 06:00 and 18:00 in a temperature-controlled environment at 25°C and humidity
234 between 40 % and 70 %, with free access to water and food. Wild type (WT) and premature
235 aging mouse models used in this study were generated by breeding (Figure S1a) and
236 housed together until they reached the desired age in the Animal Facilities of Epalinges and
237 Department of Biomedical Science of the University of Lausanne.

238

239 **Mouse strains**

240 ERCC1^{KO/Δ} 44 and XPG^{KO/KO} mice¹⁹ and littermate controls (ERCC1^{+/+} and XPG^{+/+}) were used
241 in C57BL6J|FVB hybrid background. POLG^{D257A/D257A}, herein referred to as POLG^{TG/TG} 20,21
242 and LAKI^{TG/TG} 22 and sibling controls (POLG^{+/+} and LAKI^{+/+}) were generated in C57BL6J
243 background.

244

245 **Mouse monitoring and euthanasia**

246 All mice were monitored at least three times per week to evaluate their activity, posture,
247 alertness, body weight, presence of tumors or wound, and surface temperature. Males and
248 females were euthanized at the specific timepoints by CO₂ inhalation (6 min, flow rate 20%
249 volume/min). Subsequently, before perfusing the mice with saline, blood was collected from
250 the heart. Finally, multiple organs and tissues were collected in liquid nitrogen and used for
251 DNA extraction to perform MethylArray.

252

253 **Cell culture and maintenance**

254 Human fibroblasts were obtained from the Coriell cell repositories and cultured in DMEM
255 (Gibco, 11960085) with 10% FBS (Hyclone, SH30088.03) containing non-essential amino

256 acids, GlutaMax and Sodium Pyruvate (Gibco, 11140035, 35050061, 11360039) at 37°C in
257 hypoxic conditions (3% O₂). Subsequently, fibroblasts were passaged and cultured
258 according to standard protocols.

259

260 **DNA extractions**

261 Total DNA was extracted from tissues and cells using Monarch Genomic DNA Purification
262 Kit (New England Biolab, T3010L) and protocols were carefully followed. Tissues were cut
263 into small pieces to ensure rapid lysis. Total DNA concentrations were determined using the
264 Qubit DNA BR Assay Kit (Thermofisher, Q10211).

265

266 **DNA methylation clock**

267 The mouse clock was developed in¹⁷. We used the “Pan Tissue” mouse clock since we
268 analyzed different tissues. The software code of the mouse clocks can be found in the
269 supplements of¹⁷.

270 The mouse methylation data were generated on the small and the extended version of
271 HorvathMammalMethylChip⁴⁵. We used the SeSaMe normalization method⁴⁶. Human
272 methylation data were generated on the Illumina EPIC array platforms that profiles 866k
273 cytosines. We used the noob normalization method implemented in the R function
274 preprocessNoob. The human DNAm age was estimated using the Skin&blood clock
275 algorithm²⁶.

276

277 **Statistical analysis**

278 Unsupervised hierarchical clustering based on interarray correlation coefficients was used to
279 identify putative technical outliers. One liver sample with negative methylation age was
280 removed. All plots were generated using the R software package ggplot2. Statistical
281 differences between groups were assessed using a two-tailed unpaired Student's t-test.
282 Clock performance was assessed by correlation (Pearson coefficient) and Random Mean
283 Square Error (RMSE), using the R software. To determine if there was a significant

284 difference in the slope of aging between WT and transgenic mice, we looked at the
285 significance of the interaction term in the linear regression: DNAm age ~ WT/TG + Age +
286 WT/TG*Age.

287

288 REFERENCES

- 289 1 Partridge, L., Deelen, J. & Slagboom, P. E. Facing up to the global challenges of
290 ageing. *Nature* **561**, 45-56, doi:10.1038/s41586-018-0457-8 (2018).
- 291 2 Koks, S. *et al.* Mouse models of ageing and their relevance to disease. *Mech Ageing*
292 *Dev* **160**, 41-53, doi:10.1016/j.mad.2016.10.001 (2016).
- 293 3 Liao, C. Y. & Kennedy, B. K. Mouse models and aging: longevity and progeria. *Curr*
294 *Top Dev Biol* **109**, 249-285, doi:10.1016/B978-0-12-397920-9.00003-2 (2014).
- 295 4 Bohr, V. A. Human premature aging syndromes and genomic instability. *Mech*
296 *Ageing Dev* **123**, 987-993, doi:10.1016/s0047-6374(02)00039-8 (2002).
- 297 5 Brosh, R. M., Jr. & Bohr, V. A. Human premature aging, DNA repair and RecQ
298 helicases. *Nucleic Acids Res* **35**, 7527-7544, doi:10.1093/nar/gkm1008 (2007).
- 299 6 Lopez-Otin, C., Blasco, M. A., Partridge, L., Serrano, M. & Kroemer, G. The
300 hallmarks of aging. *Cell* **153**, 1194-1217, doi:10.1016/j.cell.2013.05.039 (2013).
- 301 7 Horvath, S. DNA methylation age of human tissues and cell types. *Genome Biol* **14**,
302 R115, doi:10.1186/gb-2013-14-10-r115 (2013).
- 303 8 Simpson, D. J. & Chandra, T. Epigenetic age prediction. *Aging Cell* **20**, e13452,
304 doi:10.1111/accel.13452 (2021).
- 305 9 Ake Lu, V. P., Fei, Z., Raj, K. & Horvath, S. Universal DNA Methylation Age Across
306 Mammalian Tissues. *Innovation in Aging* **5**, 410-410,
307 doi:10.1093/geroni/igab046.1588 (2021).
- 308 10 Bell, C. G. *et al.* DNA methylation aging clocks: challenges and recommendations.
309 *Genome Biol* **20**, 249, doi:10.1186/s13059-019-1824-y (2019).
- 310 11 Bergsma, T. & Rogaeva, E. DNA Methylation Clocks and Their Predictive Capacity
311 for Aging Phenotypes and Healthspan. *Neurosci Insights* **15**, 2633105520942221,
312 doi:10.1177/2633105520942221 (2020).
- 313 12 Field, A. E. *et al.* DNA Methylation Clocks in Aging: Categories, Causes, and
314 Consequences. *Mol Cell* **71**, 882-895, doi:10.1016/j.molcel.2018.08.008 (2018).
- 315 13 Simpson, D. J., Olova, N. N. & Chandra, T. Cellular reprogramming and epigenetic
316 rejuvenation. *Clin Epigenetics* **13**, 170, doi:10.1186/s13148-021-01158-7 (2021).

- 317 14 Sarkar, T. J. *et al.* Transient non-integrative expression of nuclear reprogramming
318 factors promotes multifaceted amelioration of aging in human cells. *Nat Commun* **11**,
319 1545, doi:10.1038/s41467-020-15174-3 (2020).
- 320 15 Browder, K. C. *et al.* In vivo partial reprogramming alters age-associated molecular
321 changes during physiological aging in mice. *Nature Aging*, doi:10.1038/s43587-022-
322 00183-2 (2022).
- 323 16 Lu, Y. *et al.* Reprogramming to recover youthful epigenetic information and restore
324 vision. *Nature* **588**, 124-129, doi:10.1038/s41586-020-2975-4 (2020).
- 325 17 Mozhui, K. *et al.* Genetic loci and metabolic states associated with murine epigenetic
326 aging. *Elife* **11**, doi:10.7554/eLife.75244 (2022).
- 327 18 Weeda, G. *et al.* Disruption of mouse ERCC1 results in a novel repair syndrome with
328 growth failure, nuclear abnormalities and senescence. *Curr Biol* **7**, 427-439,
329 doi:10.1016/s0960-9822(06)00190-4 (1997).
- 330 19 Barnhoorn, S. *et al.* Cell-autonomous progeroid changes in conditional mouse
331 models for repair endonuclease XPG deficiency. *PLoS Genet* **10**, e1004686,
332 doi:10.1371/journal.pgen.1004686 (2014).
- 333 20 Kujoth, G. C. *et al.* Mitochondrial DNA mutations, oxidative stress, and apoptosis in
334 mammalian aging. *Science* **309**, 481-484, doi:10.1126/science.1112125 (2005).
- 335 21 Trifunovic, A. *et al.* Premature ageing in mice expressing defective mitochondrial
336 DNA polymerase. *Nature* **429**, 417-423, doi:10.1038/nature02517 (2004).
- 337 22 Osorio, F. G. *et al.* Splicing-directed therapy in a new mouse model of human
338 accelerated aging. *Sci Transl Med* **3**, 106ra107, doi:10.1126/scitranslmed.3002847
339 (2011).
- 340 23 Varga, R. *et al.* Progressive vascular smooth muscle cell defects in a mouse model
341 of Hutchinson-Gilford progeria syndrome. *Proc Natl Acad Sci U S A* **103**, 3250-3255,
342 doi:10.1073/pnas.0600012103 (2006).
- 343 24 Rizza, E. R. H. *et al.* Xeroderma Pigmentosum: A Model for Human Premature
344 Aging. *J Invest Dermatol* **141**, 976-984, doi:10.1016/j.jid.2020.11.012 (2021).
- 345 25 Laugel, V. in *GeneReviews((R))* (eds M. P. Adam *et al.*) (1993).
- 346 26 Horvath, S. *et al.* Epigenetic clock for skin and blood cells applied to Hutchinson
347 Gilford Progeria Syndrome and ex vivo studies. *Aging (Albany NY)* **10**, 1758-1775,
348 doi:10.18632/aging.101508 (2018).
- 349 27 Yousefzadeh, M. *et al.* DNA damage-how and why we age? *Elife* **10**,
350 doi:10.7554/eLife.62852 (2021).
- 351 28 Schumacher, B., Pothof, J., Vijg, J. & Hoeijmakers, J. H. J. The central role of DNA
352 damage in the ageing process. *Nature* **592**, 695-703, doi:10.1038/s41586-021-
353 03307-7 (2021).

- 354 29 Vermeij, W. P. *et al.* Restricted diet delays accelerated ageing and genomic stress in
355 DNA-repair-deficient mice. *Nature* **537**, 427-431, doi:10.1038/nature19329 (2016).
- 356 30 Yousefzadeh, M. J. *et al.* An aged immune system drives senescence and ageing of
357 solid organs. *Nature* **594**, 100-105, doi:10.1038/s41586-021-03547-7 (2021).
- 358 31 Mitchell, D. L. & Hartman, P. S. The regulation of DNA repair during development.
359 *Bioessays* **12**, 74-79, doi:10.1002/bies.950120205 (1990).
- 360 32 Bejaoui, Y. *et al.* DNA methylation signatures in Blood DNA of Hutchinson-Gilford
361 Progeria syndrome. *Aging Cell* **21**, e13555, doi:10.1111/accel.13555 (2022).
- 362 33 Maierhofer, A. *et al.* Accelerated epigenetic aging in Werner syndrome. *Aging*
363 (*Albany NY*) **9**, 1143-1152, doi:10.18632/aging.101217 (2017).
- 364 34 Xu, K. *et al.* Accelerated epigenetic aging in newborns with Down syndrome. *Aging*
365 *Cell* **21**, e13652, doi:10.1111/accel.13652 (2022).
- 366 35 Martin-Herranz, D. E. *et al.* Screening for genes that accelerate the epigenetic aging
367 clock in humans reveals a role for the H3K36 methyltransferase NSD1. *Genome Biol*
368 **20**, 146, doi:10.1186/s13059-019-1753-9 (2019).
- 369 36 Jeffries, A. R. *et al.* Growth disrupting mutations in epigenetic regulatory molecules
370 are associated with abnormalities of epigenetic aging. *Genome Res* **29**, 1057-1066,
371 doi:10.1101/gr.243584.118 (2019).
- 372 37 Yu, T. *et al.* Premature aging is associated with higher levels of 8-oxoguanine and
373 increased DNA damage in the Polg mutator mouse. *Aging Cell* **21**, e13669,
374 doi:10.1111/accel.13669 (2022).
- 375 38 Guastafierro, T. *et al.* Genome-wide DNA methylation analysis in blood cells from
376 patients with Werner syndrome. *Clin Epigenetics* **9**, 92, doi:10.1186/s13148-017-
377 0389-4 (2017).
- 378 39 Heyn, H., Moran, S. & Esteller, M. Aberrant DNA methylation profiles in the
379 premature aging disorders Hutchinson-Gilford Progeria and Werner syndrome.
380 *Epigenetics* **8**, 28-33, doi:10.4161/epi.23366 (2013).
- 381 40 Crochemore, C. *et al.* Epigenomic signature of the progeroid Cockayne syndrome
382 exposes distinct and common features with physiological ageing. *bioRxiv*,
383 2021.2005.2023.445308, doi:10.1101/2021.05.23.445308 (2021).
- 384 41 Meyer, D. H. & Schumacher, B. BiT age: A transcriptome-based aging clock near the
385 theoretical limit of accuracy. *Aging Cell* **20**, e13320, doi:10.1111/accel.13320 (2021).
- 386 42 Lehallier, B., Shokhirev, M. N., Wyss-Coray, T. & Johnson, A. A. Data mining of
387 human plasma proteins generates a multitude of highly predictive aging clocks that
388 reflect different aspects of aging. *Aging Cell* **19**, e13256, doi:10.1111/accel.13256
389 (2020).

- 390 43 Rechsteiner, C. *et al.* Development of a novel aging clock based on chromatin
391 accessibility. *bioRxiv*, 2022.2008.2011.502778, doi:10.1101/2022.08.11.502778
392 (2022).
- 393 44 de Waard, M. C. *et al.* Age-related motor neuron degeneration in DNA repair-
394 deficient Ercc1 mice. *Acta Neuropathol* **120**, 461-475, doi:10.1007/s00401-010-0715-
395 9 (2010).
- 396 45 Arneson, A. *et al.* A mammalian methylation array for profiling methylation levels at
397 conserved sequences. *Nat Commun* **13**, 783, doi:10.1038/s41467-022-28355-z
398 (2022).
- 399 46 Zhou, W., Triche, T. J., Jr., Laird, P. W. & Shen, H. SeSAmE: reducing artifactual
400 detection of DNA methylation by Infinium BeadChips in genomic deletions. *Nucleic*
401 *Acids Res* **46**, e123, doi:10.1093/nar/gky691 (2018).
402

Aging mouse models

bioRxiv preprint doi: <https://doi.org/10.1101/2022.12.28.522011>; this version posted December 29, 2022. The copyright holder for this preprint (which was not certified by peer review) is the author/funder, who has granted bioRxiv a license to display the preprint in perpetuity. It is made available under a [CC-BY-NC-ND 4.0 International license](https://creativecommons.org/licenses/by-nc-nd/4.0/).

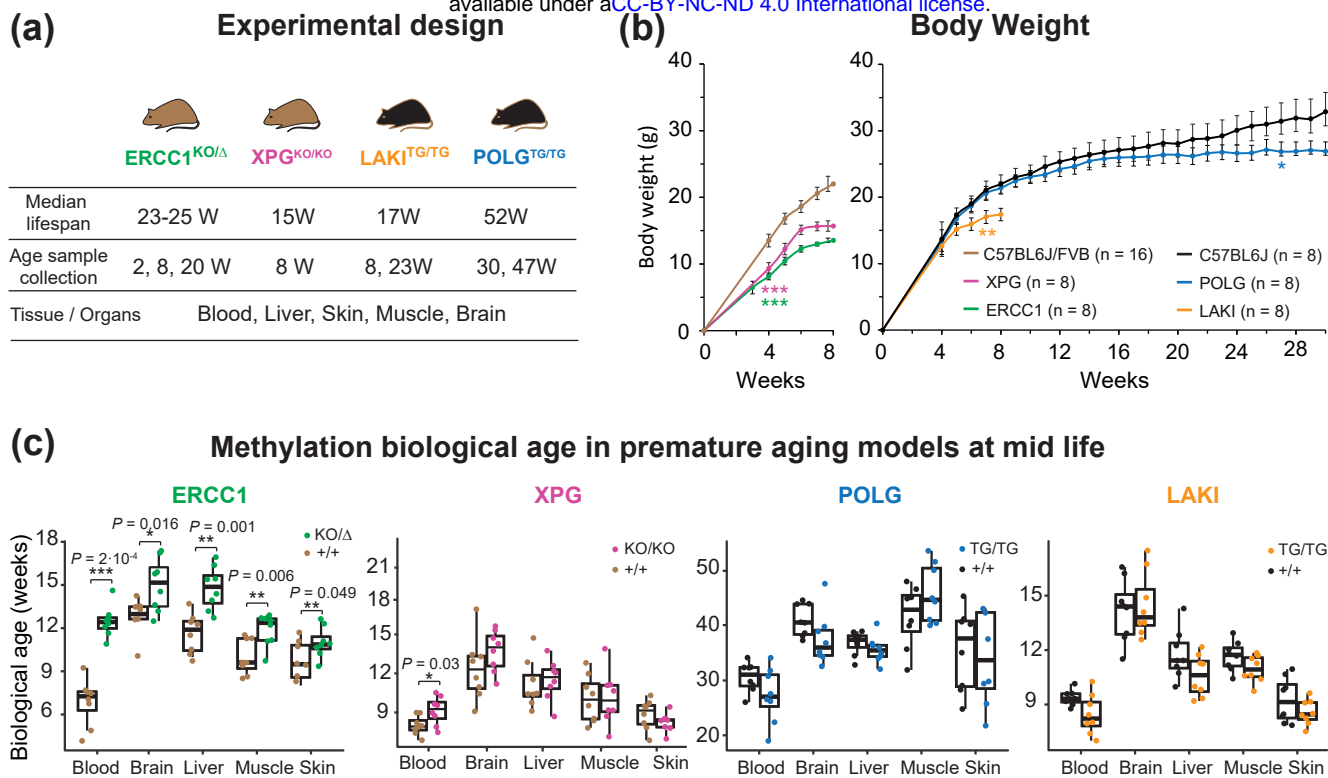


Figure 1

ERCC1 mice

bioRxiv preprint doi: <https://doi.org/10.1101/2022.12.28.522011>; this version posted December 29, 2022. The copyright holder for this preprint (which was not certified by peer review) is the author/funder, who has granted bioRxiv a license to display the preprint in perpetuity. It is made available under a [CC-BY-NC-ND 4.0 International license](#).

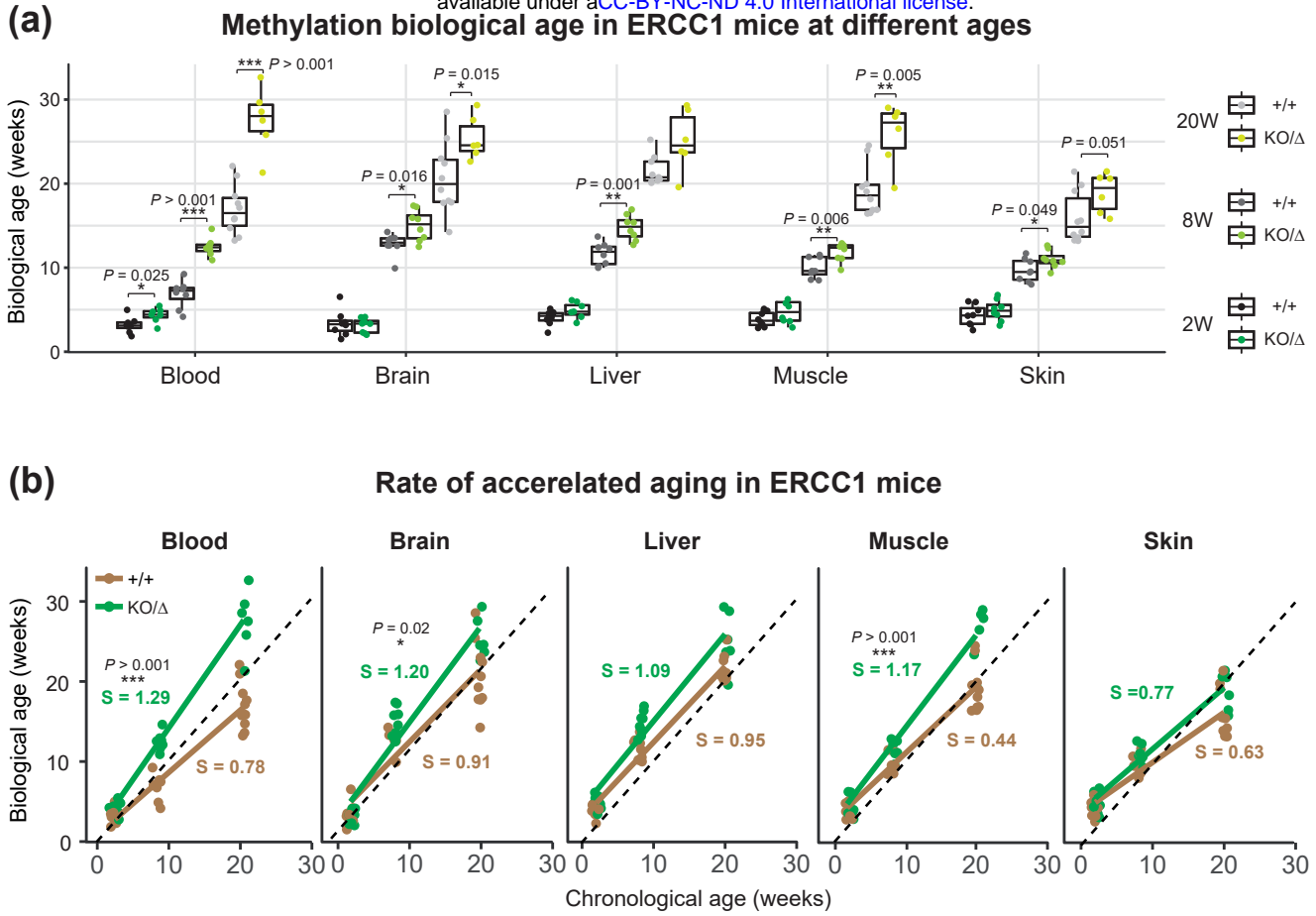


Figure 2

Human patients

bioRxiv preprint doi: <https://doi.org/10.1101/2022.12.28.522011>; this version posted December 29, 2022. The copyright holder for this preprint (which was not certified by peer review) is the author/funder, who has granted bioRxiv a license to display the preprint in perpetuity. It is made available under aCC-BY-NC-ND 4.0 International license.

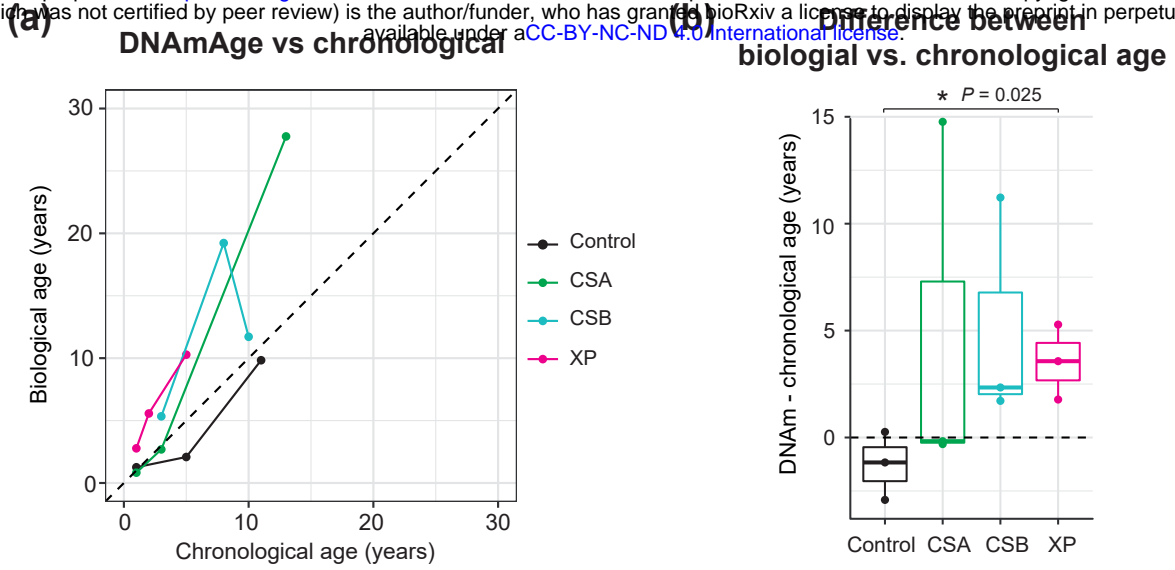


Figure 3

(a) **Generation of experimental premature aging mouse models**
 bioRxiv preprint doi: <https://doi.org/10.1101/2022.12.28.522011>; this version posted December 29, 2022. The copyright holder for this preprint (which was not certified by peer review) is the author/funder, who has granted bioRxiv a license to display the preprint in perpetuity. It is made available under aCC-BY-NC-ND 4.0 International license.

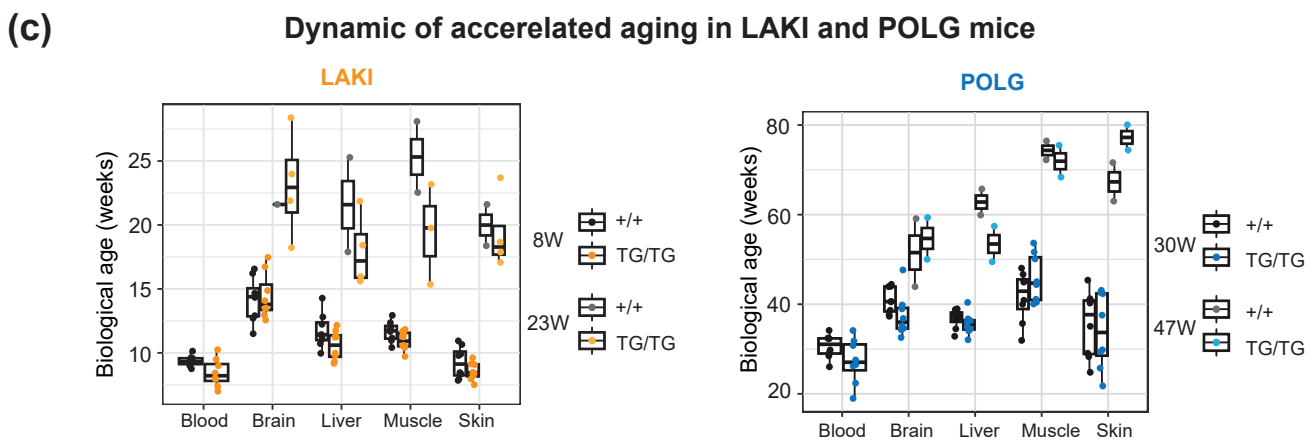
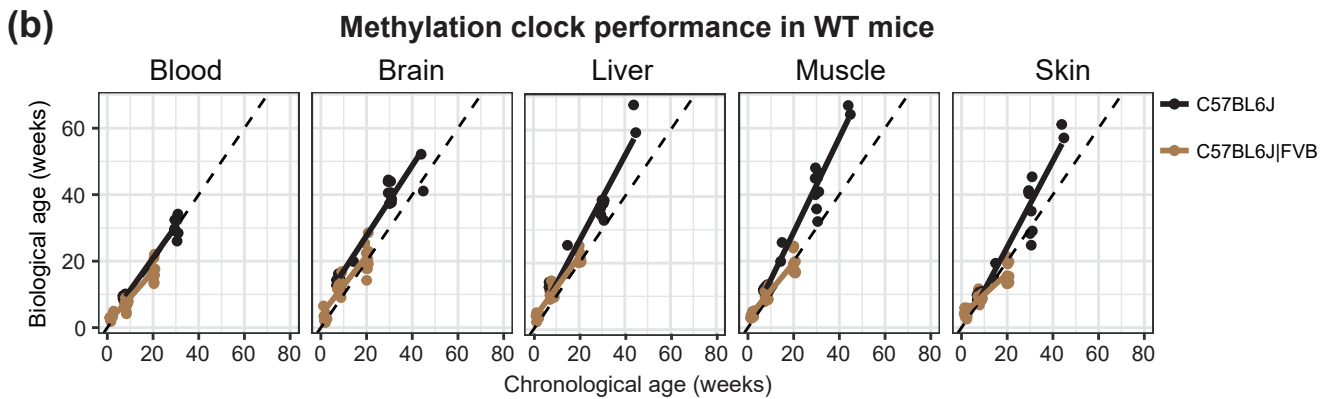
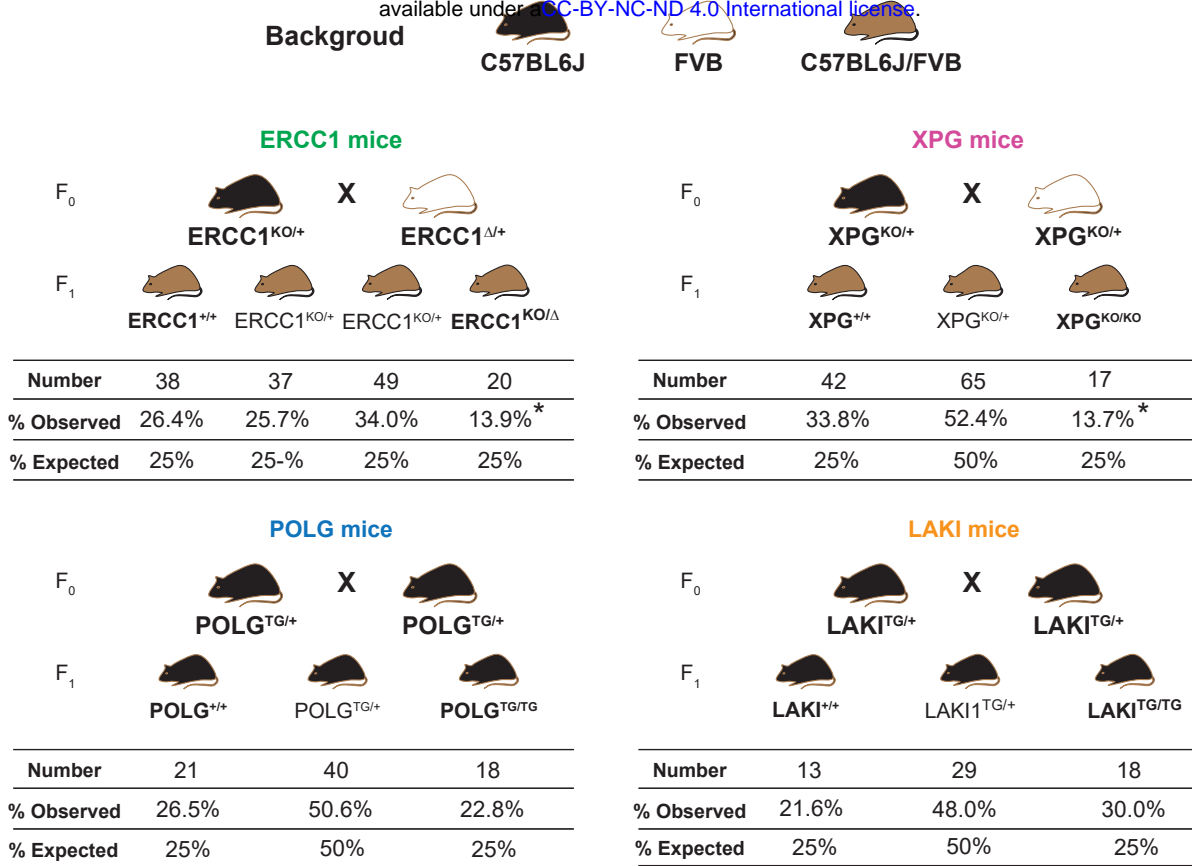


Figure S1

bioRxiv preprint doi: <https://doi.org/10.1101/2022.12.28.522011>; this version posted December 29, 2022. The copyright holder for this preprint (which was not certified by peer review) is the author/funder, who has granted bioRxiv a license to display the preprint in perpetuity. It is made available under aCC-BY-NC-ND 4.0 International license.

Tissue	C57BL6J [RMSE (r)]	C57BL6J FVB [RMSE (r)]
Blood	7.08 (0.99)	2.55 (0.95)
Brain	8.74 (0.96)	4.13 (0.89)
Liver	8.49 (0.98)	3.04 (0.97)
Muscle	11.2 (0.98)	2.51 (0.95)
Skin	7.59 (0.96)	3.21 (0.91)

Table S1

Model	Timepoint	Tissue	WT [Avg (Sd; N)]	KO [Avg (Sd; N)]	P (t-test)	Sig
ERCC1	2w	Blood	3.17 (0.93; 8)	3.55 (0.86; 7)	0.225	
		Brain	4.37 (1.53; 8)	3.12 (0.84; 8)	0.69	
		Liver	4.05 (0.9; 8)	4.89 (0.92; 7)	0.098	
	8w	Muscle	3.86 (0.88; 8)	4.75 (1.33; 8)	0.138	
		Skin	4.33 (1.25; 8)	4.91 (1.25; 8)	0.368	
		Blood	6.85 (1.62; 8)	12.46 (1.08; 8)	0	***
		Brain	12.8 (1.29; 8)	15.01 (1.84; 8)	0.016	*
		Liver	11.66 (1.33; 8)	14.78 (1.49; 8)	0.001	**
		Muscle	9.98 (1.23; 8)	11.87 (1.1; 8)	0.006	**
	20w	Skin	9.68 (1.36; 8)	11 (1.06; 8)	0.049	*
		Blood	16.95 (2.95; 10)	27.58 (3.83; 6)	0	***
		Brain	20.7 (4.23; 10)	25.39 (2.54; 6)	0.015	*
		Liver	21.56 (1.74; 9)	25.07 (3.62; 6)	0.065	
		Muscle	19.2 (2.95; 10)	25.82 (3.69; 6)	0.005	**
		Skin	15.97 (3.04; 10)	18.91 (2.37; 6)	0.051	
XPG	8w	Blood	7.96 (0.73; 8)	9.09 (1.08; 8)	0.03	*
		Brain	12.3 (2.4; 8)	13.67 (1.58; 8)	0.201	
		Liver	11.11 (1.83; 8)	11.45 (1.54; 8)	0.702	
		Muscle	10.01 (1.8; 8)	10.07 (2.04; 8)	0.947	
		Skin	8.79 (1.14; 8)	8.18 (0.7; 8)	0.22	
LAKI	8w	Blood	9.35 (0.42; 8)	8.44 (1.09; 8)	0.054	
		Brain	14.17 (1.74; 8)	14.46 (1.78; 8)	0.745	
		Liver	11.74 (1.34; 8)	10.59 (1.15; 8)	0.086	
		Muscle	11.66 (0.81; 8)	10.94 (0.74; 8)	0.085	
		Skin	9.24 (1.24; 8)	8.55 (0.69; 8)	0.199	
	23w	Brain	19.87 (NA; 1)	21.27 (3.54; 4)		
		Liver	21.13 (6; 2)	16.97 (2.31; 4)	0.501	
		Muscle	22.78 (4.04; 2)	17.92 (3.91; 3)	0.303	
		Skin	17 (3.36; 2)	15.92 (2.2; 4)	0.733	
POLG	30w	Blood	30.6 (2.68; 8)	27.3 (4.99; 8)	0.129	
		Brain	40.89 (2.93; 8)	37.5 (4.76; 8)	0.113	
		Liver	36.81 (2.15; 8)	35.63 (2.44; 8)	0.322	
		Muscle	41.67 (5.64; 8)	45.81 (5.36; 8)	0.154	
		Skin	35.6 (7.44; 8)	34.05 (8.42; 8)	0.702	
	47w	Brain	46.62 (7.83; 2)	45.96 (6.12; 2)	0.934	
		Liver	63.41 (5.88; 2)	51.25 (7.35; 2)	0.215	
		Muscle	65.48 (1.9; 2)	61.37 (6.16; 2)	0.512	
		Skin	59.1 (2.87; 2)	63.98 (1.8; 2)	0.202	

Table S2